We are IntechOpen, the world's leading publisher of Open Access books Built by scientists, for scientists

6,900
Open access books available

185,000
International authors and editors

200M
Downloads

Our authors are among the

154
Countries delivered to

TOP 1%
most cited scientists

12.2%
Contributors from top 500 universities



WEB OF SCIENCE™

Selection of our books indexed in the Book Citation Index in Web of Science™ Core Collection (BKCI)

Interested in publishing with us?
Contact book.department@intechopen.com

Numbers displayed above are based on latest data collected.
For more information visit www.intechopen.com



Chapter

Directed Self-Assembly of Block Copolymers Based on the Heterogeneous Nucleation Process

Rui Lu, Xiaobing Qu, Lu Zhang, Nana Zhu and Tao Yang

Abstract

By introducing the heterogeneous nucleation concept to directed self-assembly of block copolymers, the ordering of dynamical process and defect pattern design in thin films of binary blend, AB diblock/C homopolymer (AB/C), are investigated by the time-dependent Ginzburg-Landau theory and simulated by the cell dynamics simulations. The detailed annealing process of a few isolated defects occurring in AB/C blend under triangular and hexagonal confinements is presented, and it indicates that angle-matched confinement of triangular and hexagonal potential well is favorable conditions for generating defect-free ordered structures. Meanwhile, we gave a model which composed of many double-spot potentials with controllable position and orientation to investigate the relationship between defect spacing and mismatched angle, and we found the relationship is similar to hard crystals. Additionally, as an example, the design of defect pattern of "NXU" for abbreviation of Ningxia University is proposed and tested. In this chapter, the feasibility of directed self-assembly of block copolymers based on the heterogeneous nucleation process is systematically confirmed.

Keywords: block copolymer, directed self-assembly, heterogeneous nucleation, defect pattern, ordered pattern

1. Introduction

Moore's law is the observation that the number of transistors in a dense integrated circuit doubles approximately every 2 years [1, 2]. It means the semiconductor industry continuously pursues approaches to fabricating nanostructures with higher resolution and higher throughput at lower cost. As an important manufacturing process of semiconductor, conventional lithography is approaching its physical limit for fabricating large-scale defect-free geometrically simple patterns or device-orientated, irregular structures with sub-10 nm node [3–5]. New strategy of fabricating large-scale perfectly ordered patterns and device-orientated, interesting defect patterns via directed self-assembly of block copolymers becomes the most realistic and possible technology that is feasible to fabricate nanoimprint template to manufacture integrated circuits of semiconductor industry [6–10]. Block copolymers, a kind of macromolecules which is jointed via covalent bonds by two or more homopolymers, can self-assemble into nanoscale periodic morphologies (5–100 nm). However, the structure self-assembled by block copolymers in

bulk or in thin films on a uniform substrate is difficult to form the desired structures [11–14]. The reason is that block copolymers are typical system of soft matter; it is often interfered by thermal fluctuations resulting in the formation of uncontrollable defective morphologies. Theoretically, the defective morphologies are metastable states, and the defects would be removed as the annealing process that proceeds in a long time [15, 16]. The system would transform from metastable (disordered) state into a more stable state (ordered), that is, the system ends up in thermodynamic equilibrium state. But in fact, those defective morphologies are long-lived relative to experimentally accessible time, and the annealing time is so long that it is rare to obtain the target structure in the experiment [17–20]. Note that the system would be readily trapped kinetically into one of the many possible metastable defective states, so this process is more studied from the perspective of dynamic evolution [15, 16, 18, 21–24]. Therefore, how to overcome these shortcomings and obtain the desired target structure via self-assembly of block copolymers has become a hot topic in this field. Among the many ideas proposed by researchers, directed self-assembly (DSA) of block copolymers [6–9, 11, 12, 15, 16, 23, 24] is the most attractive scheme which has been intensively studied, and it is also regarded as a promising new-generation lithography technique [3–5, 10].

DSA is one of the most effective methods to form long-range desired patterns of block copolymer domains. The basic idea of DSA is that the small-scale pattern information is encoded into the molecular structure of block copolymers. Then, the short-range guiding patterns on the substrate from the chemical (chemoepitaxy) or topographical (graphoepitaxy) field [14, 19, 20, 25–28] could direct the orientation on long-range order and control the registration of block copolymer structures with external boundaries. Based on this concept, different geometrically confined systems, and various topographical or chemical guiding patterns on the substrate, have been devised to guide the self-assembly of block copolymers to form the desired nanostructures. For example, in AB diblock copolymer, as the macromolecular architecture changes from symmetric to asymmetric, the minor component can self-assemble into several ordered structures, such as lamellar, gyroid, Fddd network, and hexagonally arranged cylindrical, and body-centered cubic (bcc) spherical phases in the bulk [29–31]. Among those order structures, the hexagonally arranged cylindrical and lamellar phases are extensively used to prepare the samples of standing cylinders arranged in triangular lattice and geometrically stripe with line and space patterns, respectively [12, 19, 21–26, 32, 33]. Clearly, the guiding patterns must be sparse and have similar symmetries and integer multiple of periods to the domain period of the bulk phase. The density multiplication (DM) is introduced to evaluate the directing efficiency, which is defined as the ratio between the number of self-assembled domains and the number of directing substrate domains in a given area or volume of the sample. Intuitively, the sparser the guiding pattern, the lower the manufacturing cost. However, it has been proved that there exists the bottleneck in directing efficiency. The upper limit of DM in experiment for hexagonally arranged cylinders/spheres is small than 25 in the literature [12, 21, 22]. This means that the patterns on substrate could not greatly increase DM. Therefore, it remains a challenge to satisfy the rigorous demands on defect concentration and precise control required by the fabrication of integrated circuits.

Theoretically, the reason for efficiency limit is that the phase separation kinetics are spinodal microphase separation or spontaneous nucleation [34, 35]. It has an extremely high nucleation rate which induces nucleated domain grains with random positions and orientations [23]. With every domain area that grows and merges each other, the system leads to a large number of clustered defects derived from the incommensurate orientations between neighboring domain areas [15, 16].

In other words, structures formed via spinodal microphase separation cannot keep long-range order because thermal fluctuations at any locations simultaneously produce multiple grains that do not have coherent locations and orientations. Once the defects are formed, the system enters into the metastable state. As we have known, the transition from the metastable state to the stable state in block copolymer system is an extremely long process. In order to eliminate this disadvantage and increase the DM, a new DSA method, the heterogeneous nucleation, was proposed to suppress the spinodal decomposition and precisely control the domain location and orientation [15, 16, 23, 24], that is, the thermodynamics of the system must be regulated, such that the phase separation kinetics is dictated by a controlled nucleation process. These characteristics are very similar as crystals [36], so the classical nucleation theory may also be valid in block copolymers.

According to classical nucleation theory, the edges and corners of a confining system and the external nuclei can serve as heterogeneous nucleation sites with different nucleation rate [23, 35–37]. Defining the nucleation rate p, which expressed the probability of nucleation events in a unit volume per unit time, is proportional to the exponential term $\exp(-\Delta F_b/k_B T,)$, where ΔF_b is energy barrier which represents the free energy difference between certain disordered metastable phase and ordered stable phase during the first-order phase transition, k_B is the Boltzmann constant, and T is the temperature. Obviously, by controlling the nucleation rate p, the desired target structure could be obtained. Meanwhile, there are a number of promising applications in two directions with this method: (i) large-scale perfectly ordered structure by reducing homogeneous nucleation rate and controlling the location and orientation of the induced ordered domains and (ii) interesting defect patterns by optimizing the nucleation rate and programing the location and orientation of nucleation agents. The former one, which is preparation for large-scale perfectly ordered structure, has been extensively studied. Therefore, in this chapter, we only express several details of the ordering process. The latter is the main focus of our research in this chapter. We will study the properties of different defects and program the desired defect patterns by means of heterogeneous nucleation strategy, that is, designing the positions and shapes of external nuclei.

In this chapter, we select frequently used model which is thin films of binary blend, AB diblock copolymer and C homopolymer (AB/C) [15, 16, 23, 24], with a lateral confinement and neutral top and bottom surfaces. In this way, the hexagonally packed cylindrical A domains are aligned perpendicular to the substrate. Homopolymer C is often added into block copolymers to regulate the segregation degree and the domain spacing. In other words, homopolymer can adjust the homogeneous nucleation rate effectively. The kinetics of micro-/macrophase separation in this system can be described by the time-dependent Ginzburg-Landau (TDGL) theory. According to previous work, we adopt cell dynamics simulation (CDS) to solve the equations of TDGL model [15, 16, 23, 24, 38, 39].

2. Model and theory

In this system, AB/C blend, a number of parameters such as the chain lengths and interaction parameters are expressed as a series of phenomenological parameters. The volume fraction of C homopolymer is defined as $\overline{\phi}_C$, and the block ratio of the A block is f in the AB diblock copolymer. Two independent order parameters are introduced to denote the phase separation of this three-component system, $\varphi(\mathbf{r}) = \varphi_A(\mathbf{r}) - \varphi_B(\mathbf{r})$ and $\eta(\mathbf{r}) = \varphi_A(\mathbf{r}) + \varphi_B(\mathbf{r}) - \Psi_C(\mathbf{r})$, where $\varphi_A(\mathbf{r})$ and $\varphi_B(\mathbf{r})$ are the local volume fractions of A and B component at any position $\mathbf{r}$, respectively. $\Psi_C(\mathbf{r})$ is a constant that used to modulate the macrophase separation. Based on the

Ohta-Kawasaki model [38, 39] for AB/C blend, the free energy can be described as a functional of the two-order parameters,

$$F[\phi(\mathbf{r}),\eta(\mathbf{r})] = F_{\mathrm{s}}[\phi(\mathbf{r}),\eta(\mathbf{r})] + F_{\mathrm{L}}[\phi(\mathbf{r}),\eta(\mathbf{r})] + \int \mathrm{d}\mathbf{r} H_{\mathrm{ext}}(\mathbf{r})\phi(\mathbf{r}) \tag{1}$$

where F_{S} is the short-range interaction that is derived from the ordinary standard Ginzburg-Landau free energy; it is written as

$$F_{\mathrm{S}}[\phi,\eta] = \int \mathrm{dr}\left\{\frac{D_1}{2}[\nabla\phi(\mathrm{r})]^2 + \frac{D_2}{2}[\nabla\eta(\mathrm{r})]^2 + f_{\phi}[\phi] + f_{\eta}[\eta] + f_{\mathrm{int}}[\phi,\eta]\right\} \tag{2}$$

Here D_1 and D_2 are two positive constants related to the interfacial properties between the three immiscible components. The derivatives of energy density terms $f_{\phi}[\phi]$ and $f_{\eta}[\phi]$ are given by $\frac{\mathrm{d}f_{\phi}[\phi]}{\mathrm{d}\phi} = -A_{\phi}\tan\phi + \phi$ and $\frac{\mathrm{d}f_{\eta}[\eta]}{\mathrm{d}\eta} = -A_{\eta}\tan\eta + \eta$ with $A_{\phi} > 1$ and $A_{\eta} > 1$ to tune the micro-/macrophase separation degree. The last term is expressed as $f_{\mathrm{int}} = b_1\eta\phi - \frac{b_2\eta\phi^2}{2} - b_3\left(\eta\phi^3 + \eta^2\phi + \eta^3\phi\right) + \frac{b_4\eta^2\phi^2}{2}$, where the phenomenological coefficients $b_i (i = 1, 2, 3, 4)$ is constant with unambiguous physical meaning as proposed by Ohta and Ito.

The long-range interaction term F_{L} is expressed as

$$F_{\mathrm{L}}[\phi,\eta] = \int \mathrm{dr}\int \mathrm{dr}' G(\mathrm{r},\mathrm{r}')\left[\frac{\alpha\delta\phi(\mathrm{r})\delta\phi(\mathrm{r}')}{2} + \beta\delta\phi(\mathrm{r})\delta\eta(\mathrm{r}') + \frac{\gamma\delta\eta(\mathrm{r})\delta\eta(\mathrm{r}')}{2}\right] \tag{3}$$

where $\delta\phi(\mathbf{r}) = \phi(\mathbf{r}) - \overline{\phi}$ and $\delta\eta(\mathbf{r}) = \eta(\mathbf{r}) - \overline{\eta}$ and $\overline{\phi}$, $\overline{\eta}$ are average values in full space for $\phi(\mathbf{r})$ and $\eta(\mathbf{r})$, respectively. The coefficients α, β and γ are related to the polymerization degrees of AB and C, which obey the relationship of $\frac{\beta}{\alpha} = \frac{\gamma}{\beta}$. The Green function of $G(\mathbf{r},\mathbf{r}')$ is with a Coulomb interaction form that denotes the long-range feature of the chain connectivity of the diblock copolymer. In the last term of free energy in Eq. (1), $H_{\mathrm{ext}}(\mathbf{r})$ is a potential field imposed on nucleation agent whose explicit expression will be given in the following sections for different models.

The phase separation kinetics of AB/C blend is dominated by following two conserved Cahn-Hilliard equations:

$$\frac{\partial\phi}{\partial t} = \frac{M_1\nabla^2\delta F[\phi,\eta]}{\delta\phi} + \xi_{\phi}(\mathrm{r},t) \tag{4}$$

$$\frac{\partial\eta}{\partial t} = \frac{M_2\nabla^2\delta F[\phi,\eta]}{\delta\eta} + \xi_{\eta}(\mathrm{r},t) \tag{5}$$

where M_1, M_2 are two mobility coefficients and ξ_{ϕ}, ξ_{η} are the random noise terms that satisfy the fluctuation dissipation theorem. For the sake of discussion, the parameters of system are set as $f = 0.4$, $D_1 = 0.5$, $D_2 = 1$, $M_1 = M_2 = 1$, $A_{\phi} = 1.26$, $A_{\eta} = 1.10$, $b_1 = -0.05$, $b_2 = 0.05$, $b_3 = 0.01$, $b_4 = 0.10$, $\Psi_C = 0.20$, and $\overline{\phi}_{\mathrm{C}}$ is fixed as $\overline{\phi}_{\mathrm{C}} = 0.025$. All spatial lengths in the following calculations are expressed in terms of the cylinder-to-cylinder distance L_0 in AB/C blend. Because this model is the thin films of binary blend, the system is simplified to be two-dimensional; hence the hexagonally packed cylindrical A domains would align perpendicular to the substrate. The kinetic equations can be solved numerically by standard discretization scheme of CDS. Based on CDS, the two-dimensional substrate is divided into $N_x \times N_y$ squares with length of its sides $\Delta x = \Delta y = \Delta = 0.5$, and the Laplace operator is written as

$$\nabla^2 X = \left(\frac{1}{6}\sum_{nn} X_i + \frac{1}{12}\sum_{nnn} X_i - X\right)/\Delta^2 \tag{6}$$

where "nn" denotes nearest neighbors and "nnn" next-nearest neighbors.

3. Results and discussion

3.1 Phase-ordering process

It has been proved that the large-scale perfectly ordered hexagonal patterns can be obtained by many block copolymer systems with different DM. Early experiments and theories indicated that the maximum DM would not exceed 25 [12, 21, 22], and later it was increased to 34 confirmed by self-consistent mean field theory [40]. Recently, a very innovative idea has been proposed by Xie et al. [23], which greatly improves the directing efficiency. The idea is based on the concept of heterogeneous nucleation. By careful adjustment of the sparse periodic array of several pairs of potential wells in AB/C blend, it realized perfect hexagonal pattern with DM values of at least 128. However, this scheme has serious shortcomings in manufacture process because the nucleation agent unit size is as small as the lattice constant L_0. Thus, other nucleation agents are needed. Inspired by the classical nucleation theory, the six corners of lateral hexagonal confinement would be an ideal choice [24]. Corner-induced domain grains grow and integrate into an ordered hexagonal pattern filling in whole substrate. Because the corner angle is 120°, which is commensurate in hexagonal pattern, this method is high-efficient. Because this method is ready to implement, Ho et al. [41] realized a defect-free hexagonal pattern by self-assembly of star-block PS–PDMS based on heterogeneous nucleation. Although the hexagonal confinement is not difficult to produce technically, there is a better choice, such as rectangular confinement. Yang et al. [15] demonstrated the heterogeneous nucleation process in rectangular confinement and still acquired the defect-free hexagonal pattern.

Most of the above work focuses on the implementation of perfectly ordered hexagonal patterns and rarely gives the ordering process after growth time t_{fill} which denotes the moment when domains grow up to fill in the entire sample. However, the ordering process is very important in the sample preparation of lithography techniques. The size and shape of confinements, the position and orientation of nucleation agents, the strength and range of chemical potential, and so on all severely affect the path of phase-ordering kinetics from a metastable disordered phase to ordered phase. Here we will give this process in detail. Considering the angle-matched confinement that will lead to ordered structure, we choose lateral, triangular, and hexagonal confinements to demonstrate the process.

Since AB/C blend is laterally confined in triangular and hexagonal well, an external field, $H_{\text{ext}}(\mathbf{r})$ is imposed on each sidewall to denote the preferential interaction on A or B block; and thus the sidewalls are acted as nucleation agents. The form of field is set as

$$H_{\text{ext}}(\mathrm{r}) = \frac{1}{2}\Lambda_0\left\{\tanh\left[\frac{\sigma - d(\mathrm{r})}{\epsilon}\right] + 1\right\} \tag{7}$$

where the shortest distance of the position $\mathbf{r}$ to any sidewall is $d(\mathbf{r}) < 2\sigma$. In Eq. (7), Λ_0 is the field strength, 2σ is the interaction distance, and ϵ is the potential steepness, respectively. For convenience, here we fixed $\sigma = 0.15L_0$, $\epsilon = 0.5L_0$ in following calculations, and more details can be found elsewhere [15, 24].

It is worth noting that in the process on DSA of block copolymer, the defects are inevitable. When angle-matched confinement is introduced, a number of isolated dislocations (or five-seven defect pairs) are occurred due to the thermal fluctuations. In theory and experiment, the dislocations would be annihilated in long time. In **Figure 1**, the defect annealing process which started as the growth time t_{fill} under triangular confinement is presented.

As can be seen from **Figure 1a**, there are five dislocations when the phase separation just finished and the domains were filled in the sample at $t = t_{\text{fill}} = 3.5 \times 10^5$. With the continuous evolution process, all defects gradually moved in the direction of their nearest side and at $t = 1.0 \times 10^6$; the defect in the lower left corner has disappeared, which is shown in **Figure 1b**. Obviously, all defects are constantly moving outward in order to transform into a more steady state. In **Figure 1c**, the defect on the right side is eliminated by annealing at $t = 3.0 \times 10^6$, and at this stage, only three five-seven defect pairs remain in whole substrate. Until $t = 1.0 \times 10^7$ in **Figure 1d**, the number of defects did not decrease, but the distance between them increased, and all defects are closer to the sides. This annealing process also shows that the relaxation time of soft matter system is extremely long.

Additionally, we also considered the long-time annealing behavior under the hexagonal confinement. In **Figure 2a**, there are four isolate five-seven dislocations and four isolate seven disclinations in sample. When the domain nucleated from each angle and the domain area expanded and intersected each other at the center of the edge, the distance between the cylinders is more than one time of L_0, so a disclination may be formed at four sides. The two defects that are closer to the top and the bottom sides are different from the other four disclinations at sides, which may derive from the algorithm and we will discuss later. After a long time, in **Figure 2b**, by adjusting its period, even if it is slightly larger than L_0, the system gradually evolves to a steady state, thus the four disclinations are eliminated. In **Figure 2c**, the two five-seven dislocations in the center of the sample, because they

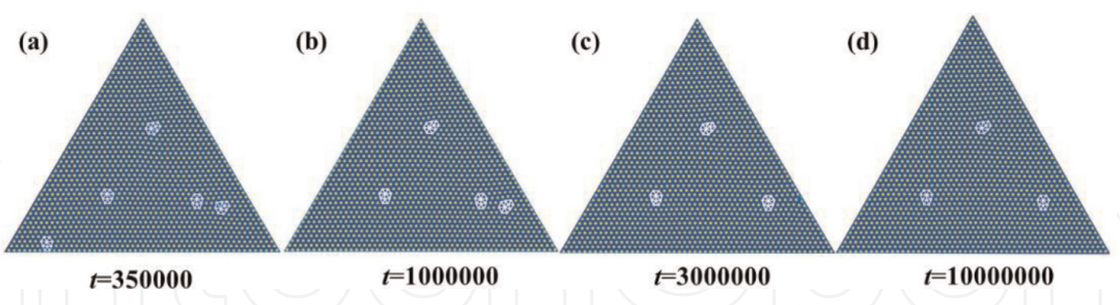


Figure 1.
Snapshots of a few side-induced five-seven dislocations observed during the annealing process (a)–(d) formed in triangular confinement with field strength $\Lambda_0 = 0.005$ and a side length $L = 50.5L_0$.

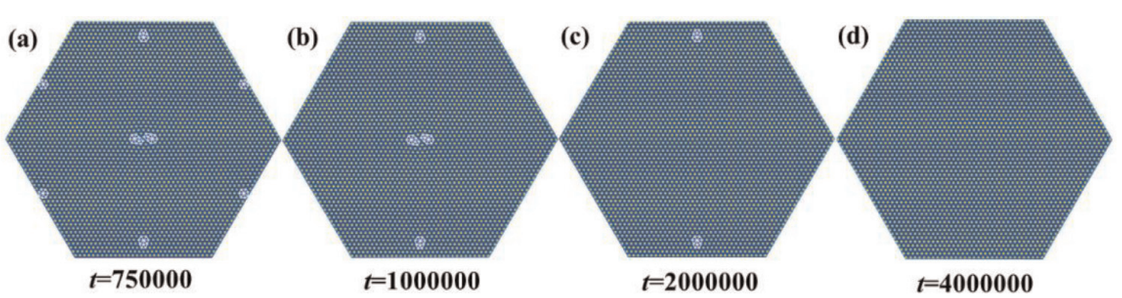


Figure 2.
Snapshots of a few side-induced five-seven dislocations observed during the annealing process (a)–(d) formed in hexagonal confinement with field strength $\Lambda_0 = 0.003$ and a side length $L = 30.5L_0$.

have nearly opposite Burgers vectors, move toward each other and finally cancel each other. Similarly, the two remaining defects move in the direction of sides and are annihilated. Finally, a defect-free pattern is obtained in **Figure 2d**.

It is worth noting that the phase-ordering kinetics given in **Figures 1** and **2** describes the process from a disordered metastable state to an ordered stable state. On the one hand, from the perspective of energy, the defect annealing process is also the process of releasing stress energy and reducing free energy of the system [42, 43]. On the other hand, the angle-matched confinement with triangular and hexagonal well is favorable conditions for generating defect-free ordered structures.

The other one is worth noting that the size commensurability or size tolerance of the directing effect to the confinement is very important. In general, the spacing of domains self-assembled by the block copolymer with a certain confinement is adjusted itself within a limited range to obtain ordered structure. However, when the size is incommensurate with the domain spacing, it is very difficult to form defect-free structure. The defect concentration is introduced to evaluate the direct efficiency, which is defined as $f_{\mathrm{DF}} = \frac{n_{\mathrm{DF}}}{n_{\mathrm{domain}}} \times 100\%$, where n_{domain} is the total number of domains and n_{DF} the number of five-seven dislocations in the sample.

In previous work, it has been proved that there is a size tolerance window for manufacture of large-scale ordered structures via the heterogeneous nucleation process in the hexagonal and rectangle confinements. In other words, the directing effect is dependent on the geometric confinement size, even for the angle-matched hexagonal confinement. But it is amazing that there is no size dependent for regular triangular confinement systems when nucleation is corner-induced with a weak field $\Lambda_0 = 0.002$. In **Figure 3**, the average concentrations $<f_{\mathrm{DF}}>$ calculated by averaging 10 independent runs are shown. When the system is corner-induced ($\Lambda_0 = 0.002$), the defect concentrations $<f_{\mathrm{DF}}>$ keep zero with the size length from $10L_0$ to $55L_0$. While the size length L increases to $55L_0$, more than 1300 cylinder domains are contained in the sample, and the system has reached the μm scale. This intriguing feature contrasts with existing work and would have potential

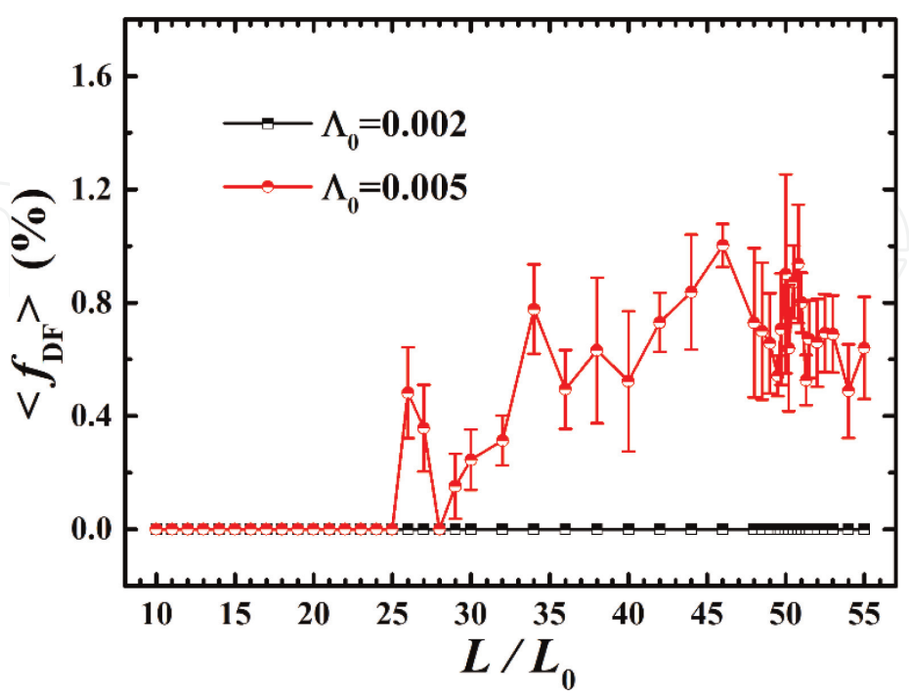


Figure 3.
Average defect concentration of the hexagonal pattern $<f_{\mathrm{DF}}>$ as a function of side length L for field strength $\Lambda_0 = 0.002$ and 0.005. The point value and its standard deviations are obtained by averaging the data on 10 independent simulation samples.

applications in the manufacture of integrated circuits. Under a slightly stronger field, $\Lambda_0 = 0.005$, the defect concentration $<f_{DF}>$ is zero at small size sample and is with a small fluctuation amplitude within $0 \leq <f_{DF}> \leq 1.2\%$ at larger size because of high probability of defects that still has no obvious limit to the size. As is known, the mismatched angle between neighboring domain grains is multiples of 60°; the two grains may merge into a single crystalline grain. Here the regular triangular system is just the smallest multiples of 60°; compared to hexagonal system, 120°, it has strong confining effect and thus has higher tolerance to the size incommensurability.

3.2 Spacing of dislocations

Based on the concept of heterogeneous nucleation [36], different boundary conditions acted as nucleating agents and can be introduced, such as the corners and sides of different geometric confinements. The defect-free hexagonal patterns can be realized. However, due to the common irregular structures in the semiconductor industry, the same attention should be paid to the defect as to ordered structures in block copolymers.

The large-scale regular/irregular soft crystal structures formed from DSA of block copolymers are fundamentally different from those conventional crystals. The defects or dislocations in this soft crystal may have distinctive features as to those in hard crystals. But we might study and understand some property of soft matter with the help of classical nucleation theory. According to classical nucleation theory, the average distance between dislocations is related to the mismatched angle between neighboring domain grains. As shown in **Figure 4a**, taking two hexagons, the axis of one hexagon is horizontal, and the other one is tilted θ relative to the horizontal axis. In this way, the two domain grains are at a mismatched angle of θ, resulting in defects when θ is not multiples of 60°. Intuitively, different angles correspond to different overlap areas of two hexagons; thus we first investigate the overlapping area for convenience. In **Figure 4a**, the shaded area APRQA is one-sixth of the whole overlap areas, and the area is expressed as

$$S_{OL} = 6S_1 = 6\left(\int_0^{x_Q} y_{AQ}dx + \int_{x_Q}^{x_R} y_{CD}dx + \int_{x_R}^{x_P} y_{BE}dx - \int_{x_P}^{0} y_{AP}dx\right) \tag{8}$$

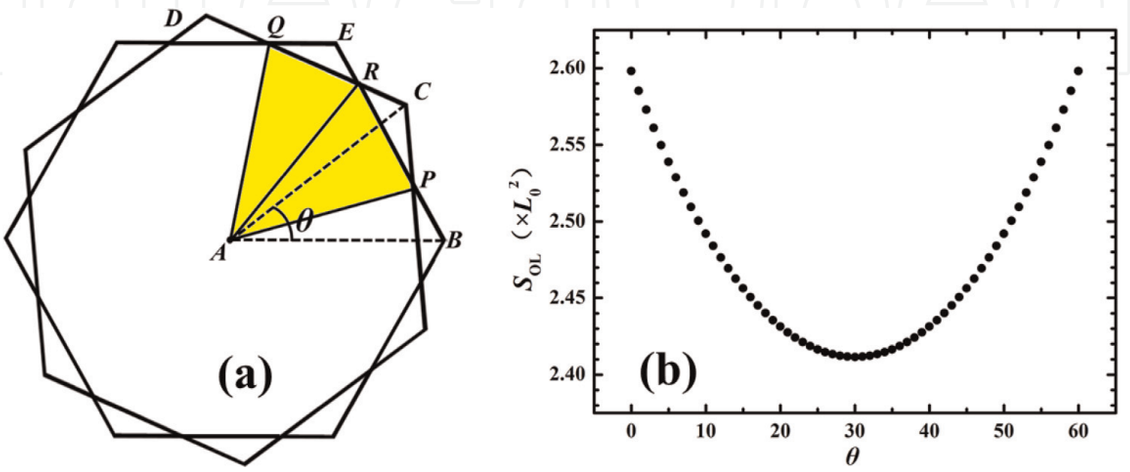


Figure 4.
(a) Schematic representation of overlapping region of two hexagons. The axis of one hexagon is horizontal, and the other is tilted θ relative to the horizontal axis, and the shaded area marks one-sixth of the overlap area. (b) The overlap area varies with mismatched angle θ of the two hexagons.

where $y_{AQ}, y_{CD}, y_{BE}, y_{AP}$ are functional expressions for line AQ, CD, BE, and AP in coordinate system. The coordinate system is established as follows: the center of the hexagons is the origin, the horizontal right direction is the positive direction of the x-axis, and the vertical upward direction is the positive direction of the y-axis. Specifically, $y_{AQ} = 3\left[\sec\left(\frac{\pi}{6}+\theta\right) - \tan\frac{\pi}{6}+\theta\right]x, y_{CD} = -\cot\left(\frac{\pi}{6}+\theta\right)x + \sin\theta + \cot\left(\frac{\pi}{6}+\theta\right)\cos\theta, y_{BE} = -\sqrt{3}x + \sqrt{3}, y_{AP} = \left(2-\sqrt{3}\right)x$, and the side length of hexagons is formally fixed as L_0. The results are shown in **Figure 4b**.

Figure 4b shows the relationship between the overlap area and mismatched angle. When $\theta \to 0$, the two hexagons coincide each other, so the overlap area is maximized. In another words, the mismatch degree is zero at $\theta \to 0$, so there are no defects in sample. As θ increases, the overlap area gradually decreases, and the minimum value is reached when $\theta = 30^{\circ}$. In this process, the mismatch degree increases gradually and finally reaches the maximum, which means that the number of defects also increase, that is, the dislocations arrange from sparse distribution to the closest arrangement. In contrast, the overlap area increases again after $\theta = 30^{\circ}$, until $\theta = 60^{\circ}$. This law is similar to that of the distance between defects in hard crystals.

In order to validate this relationship, we propose a model in which two domain grains are induced by two pairs of double-spot potential. The schematic is shown in **Figure 5**. Using the double-spot potential as the nucleation agents, the domain grain with definite orientation can be produced. In **Figure 5**, each pair of the double well is tilted $\frac{\theta}{2}$ relative to the horizontal axis; thus the angle between the two domain grains induced by them is θ. The two grains start to grow from double well and will meet in the middle of the two wells ($y = \frac{L_y}{2}$) and finally get a number of five-seven dislocations if the mismatched angle will not be multiples of 60°. By examining the distance of dislocations produced by this model, the relationship between mismatched angle θ and average spacing of dislocations d_{DL} will be calculated quantitatively. The morphological snapshots of five-seven dislocations at different mismatched angle θ are presented in **Figure 6**.

As a nucleation agent, the double-spot potential spaced at equal distance L_0 as shown in **Figure 5** can orient the induced ordered domains. Therefore, we put a potential field with the following form around double spots [23]:

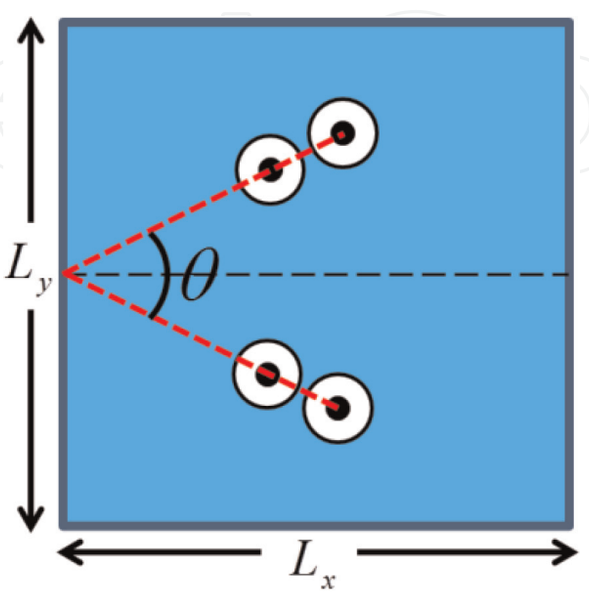


Figure 5.
Schematic of the setup for preparation of two domain grains. The nucleation agent is composed of two pairs of double-well potentials, of which each pair is tilted $\frac{\theta}{2}$ relative to the horizontal axis.

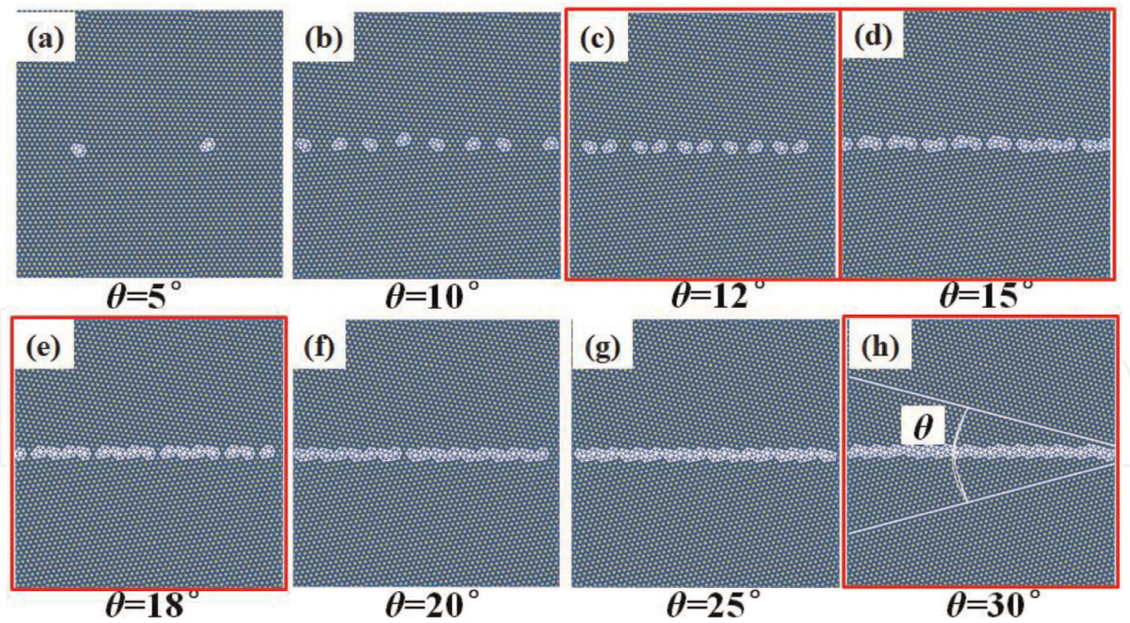


Figure 6.
Morphological snapshots of five-seven defect pattern at different mismatched angle θ of two domain grains. From (a) to (h), θ = 5, 10, 12, 15, 18, 20, 25, 30°. We fixed the size of sample $50L_o \times 50L_o$ and the position of the two double-spot wells that are selected at $\left(\frac{L_x}{2}, \frac{L_y}{6}\right)$ and $\left(\frac{L_x}{2}, \frac{5L_y}{6}\right)$, respectively. The marked in red (c), (e), (d), and (h) represent that AB/C blend is under the regular pentagonal (corner- and side-induced), octagonal, and square confinements.

$$H_{\text{ext}}(\mathrm{r}) = -\frac{V_0}{2}\left\{\tanh\left[\frac{-|\mathrm{r} - R_n| + \sigma}{\lambda}\right] + 1\right\} \tag{9}$$

for $|\mathbf{r} - \mathbf{R}_\mathrm{n}| \leq 2\sigma$ and otherwise $H_{\text{ext}}(\mathbf{r}) = 0$. The strength of field $V_0 = 0.04$ denotes that the spot potential is preferential to minor component A block. $\mathbf{R}_\mathrm{n}$ indicates the coordinate of spot potential n, and $\sigma = 0.15L_0$ is the radial size of well, and $\lambda = 0.5$ gives the steepness of potential well.

In **Figure 6**, we select square confinement with fixed boundary conditions, and the size of sample is $50L_0 \times 50L_0$. The centers of two double-spot potentials are set at center in the x direction, symmetric with respect to $= \frac{L_y}{2}$, that is, $\left(\frac{L_x}{2}, \frac{L_y}{6}\right)$ and $\left(\frac{L_x}{2}, \frac{5L_y}{6}\right)$; thus they can induce two pieces of ordered domain grains which meet at $\frac{L_y}{2}$ due to the symmetry. When the two grains have different orientations, a few five-seven dislocations are formed at $\frac{L_y}{2}$.

Because the above setup can be used to investigate the defect distribution under continuous change of mismatched angles, we only give eight typical morphological snapshots of five-seven dislocations at $\theta = 5, 10, 12, 15, 18, 20, 25, 30^\circ$ in **Figure 6a–h**. It is worthy noted that when $\theta = 0^\circ$, an ordered structure is obtained because of same orientations for two grains induced by the two double-spot potentials. It also indicates the spacing of dislocations $d_{\text{DL}} \to \infty$ when $\theta = 0^\circ$. With the increase of the mismatched angle θ, more and more dislocations are formed where the domain grains meet. Accordingly, the spacing of dislocations is decreasing, and the dislocations are arranged more and more closely, as shown in **Figure 6a–g**. When $\theta = 30^\circ$, the distance of dislocations is minimized, and the five-seven dislocations are end-to-end (**Figure 6h**). This result is consistent with that of **Figure 4**. So, the relationship for spacing of dislocations in hard materials may hold for this system whose units are soft deformable domains and are very distinguishable from atoms. Here is the relationship between mismatched angle and distance of dislocations [16, 36, 42–45],

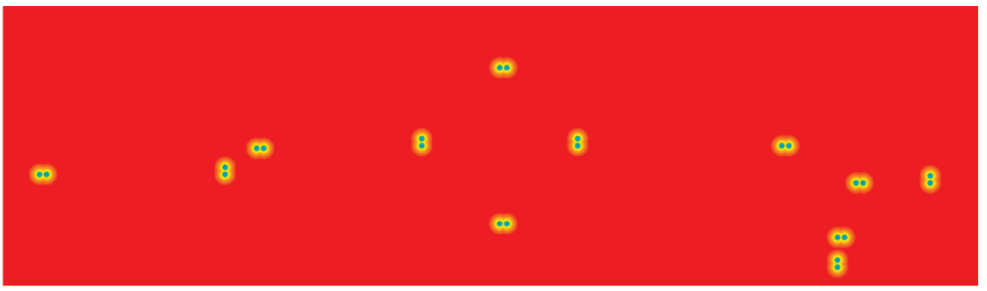


Figure 7.
Snapshots of distribution of 12 nuclei which composed of the double-spot potential. The size of sample is $120L_0 \times 40L_0$.

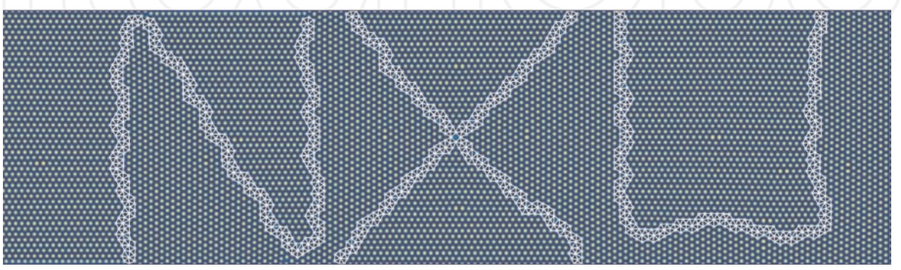


Figure 8.
Snapshots of defect pattern "NXU" formed via heterogeneous nucleation process originated from ***Figure 7****.*

$$d_{\mathrm{DL}} \propto \frac{a_0}{2\sin\left(\frac{\theta}{2}\right)} \tag{10}$$

where a_0 is the lattice constant and in this soft crystal system $a_0 = L_0$.

Although the above discussions focus on the properties of dislocations, they also provide us with a new idea that dislocations are controllable with heterogeneous nucleation technique. One on hand, nucleation agents with desired positions and uniform orientation can make single-crystal pattern efficiently because of no defect occurring at this condition. On the other hand, by tailoring the positions and orientations of nucleation agents, we can program the defect patterns in soft crystals and obtain the devise-oriented irregular structures which might have potential applications in metamaterials, semiconductor industry, etc.

3.3 Defect patterns

As well as we known, a significant feature of soft matter is sensitively responsive to thermal fluctuations as well as external fields. In these systems, the contribution of entropy is not negligible and even more important than the contribution of enthalpy. Therefore, the probability of formation of defects increases dramatically because of the responsiveness to thermal fluctuations. Conversely, the opportunities to design soft crystals are offered, such as fabrication of large-scale order structures and devise-oriented irregular structures, because of their sensitive responsiveness to external fields.

In Section 3.2, we have already discussed the properties of dislocations in detail and have proposed a feasible technique to obtain the desired pattern by controlling the nucleation process. The technique is originated from the concept of heterogeneous nucleation. Using this method, we give a design scheme to implement a defect pattern of "NXU" which is abbreviation for Ningxia University.

We choose the size of the two-dimensional sample as $120L_0 \times 40L_0$ with fixed boundary conditions. Many nuclei composed of the double-spot potential are put in designed positions and orientations. The parameters are the same as in Section 3.2.

Specifically, the positions and orientations of nuclei are shown in **Figure 7**. For convenience, we only selected two double-spot orientations that were standing at 0and 90° to the horizontal direction. This means that the grains induced by them either would be commensurate with each other ($\theta = 0$) and formed an ordered structure or produce the densest defects ($\theta = 30^{\circ}$) when they meet.

The final defect pattern induced by the nucleus agent distributed in **Figure 7** is shown in **Figure 8**. As we expected, the desired pattern "NXU" is obtained. It proves the feasibility of the technique for producing desired patterns via a heterogeneous nucleation process in block copolymers. In principle, most of the irregular patterns at the nanoscale can be obtained by this method.

4. Conclusions

In block copolymers, as a typical system of soft matter, the kinetic and thermodynamic behaviors are sensitively responsive to thermal fluctuations and external fields. The pattern self-assembled by block copolymers is inevitable to face this problem. In order to produce desired pattern, an effective technique of DSA via heterogeneous nucleation is adopted to investigate the behaviors of self-assembly. Two potential applications are considered by the method in this chapter. One is the phase-ordering process, and the other is the defect pattern design. The corresponding process of thin films of binary blend, AB diblock copolymer, and C homopolymer is simulated using the CDS based on the TDGL, demonstrating the feasibility and practicality of heterogeneous nucleation in fabrication of desired nanoscale patterns.

Because there are many factors that affect the self-assembly process, the phase-ordering process is very important in the sample preparation of lithography techniques. By adjusting the heterogeneous nucleation process, the path of phase-ordering kinetics from a metastable disordered phase to ordered phase is easier to achieve. We choose two angle-matched confinements, lateral triangular and hexagonal confinements, whose sides and corners are acted as nucleation agents, to demonstrate the phase-ordering process. Especially, the annealing process for a small number of defects was also recorded. It may be useful for the preparation of large-scale ordered structures.

On the contrary, irregular structures with various defect patterns in the semiconductor industry have received little attention. However, the study for defect in soft matter is of great significance both theoretically and experimentally, because of so many distinctive features for soft matter as to those in hard crystals. We gave a robust model which composed of many double-spot potentials with controllable position and orientation, to investigate the relationship between defect spacing and mismatched angle. Additionally, as an example, the design of defect pattern of "NXU" for abbreviation of Ningxia University is proposed.

With the development of DSA techniques via heterogeneous nucleation process, various defect-free patterns on large scales or irregular device-oriented structures are technically easy to implement. In order to obtain more complex structures or structures with smaller characteristic dimensions, more efforts should devote to optimizing the properties and extending the choice of materials in theory and experiment.

Acknowledgements

Rui Lu thanks the funding support by the National College Students' innovation and entrepreneurship training program (Grant No. 201810749005).

T.Y. thanks the funding support by the Natural Science Foundation of Ningxia (Grant No. NZ1640).

Conflict of interest

The authors have no conflict of interest to declare.

IntechOpen

IntechOpen

Author details

Rui Lu, Xiaobing Qu, Lu Zhang, Nana Zhu and Tao Yang*
Ningxia Key Laboratory of Information Sensing and Intelligent Desert, School of Physics and Electronic-Electrical Engineering, Ningxia University, Yinchuan, China

*Address all correspondence to: yang_tao@alumni.sjtu.edu.cn

IntechOpen

© 2019 The Author(s). Licensee IntechOpen. This chapter is distributed under the terms of the Creative Commons Attribution License (http://creativecommons.org/licenses/by/3.0), which permits unrestricted use, distribution, and reproduction in any medium, provided the original work is properly cited. CC BY

References

[1] Moore GE. Cramming more components onto integrated circuits. Proceedings of the IEEE. 1998;**86**:82-85. DOI: 10.1109/JPROC.1998.658762

[2] Gelsinger P. Moore's law—The genius lives on. IEEE Solid-State Circuits Newsletter. 2006;**20**:18-20. DOI: 10.1109/N-SSC.2006.4785855

[3] Park M, Harrison C, Chaikin PM, Register RA, Adamson DH. Block copolymer lithography: Periodic arrays of ~1011 holes in 1 square centimeter. Science. 1997;**276**:1401-1404. DOI: 10.1126/science.276.5317.1401

[4] Cheng JY, Ross CA, Thomas EL, Smith HI, Vancso GJ. Fabrication of nanostructures with long-range order using block copolymer lithography. Applied Physics Letters. 2002;**81**: 3657-3659. DOI: 10.1063/1.1519356

[5] Stoykovich MP, Müller M, Kim SO, Solak HH, Edwards EW, de Pablo JJ, et al. Directed assembly of block copolymer blends into nonregular device-oriented structures. Science. 2005;**308**:1442-1446. DOI: 10.1126/science.1111041

[6] Darling SB. Directing the self-assembly of block copolymers. Progress in Polymer Science. 2007;**32**:1152-1204. DOI: 10.1016/j.progpolymsci.2007.05.004

[7] Herr DJC. Directed block copolymer self-assembly for nanoelectronics fabrication. Journal of Materials Research. 2011;**26**:122-139. DOI: 10.1557/jmr.2010.74

[8] Luo M, Epps TH III. Directed block copolymer thin film self-assembled: Emerging trends in nanopattern fabrication. Macromolecules. 2013;**46**: 7567-7579. DOI: 10.1021/ma401112y

[9] Hu H, Gopinadhan M, Osuji CO. Directed self-assembly of block copolymers: A tutorial review of strategies for enabling nanotechnology with soft matter. Soft Matter. 2014;**10**: 3867-3889. DOI: 10.1039/C3SM52607K

[10] Bates CM, Maher MJ, Janes DW, Ellison CJ, Willson CG. Block copolymer lithography. Macromolecules. 2014;**47**: 2-12. DOI: 10.1021/ma401762n

[11] Li WH, Müller M. Defects in the self-assembly of block copolymers and their relevance for directed self-assembly. Annual Review of Chemical and Biomolecular Engineering. 2015;**6**: 187-216. DOI: 10.1146/annurev-chembioeng-061114-123209

[12] Bita I, Yang JKW, Jung YS, Ross CA, Thomas EL, Berggren KK. Graphoepitaxy of self-assembled block copolymers on two-dimensional periodic patterned templates. Science. 2008;**321**:939-943. DOI: 10.1126/science.1159352

[13] Campbell IP, Lau GJ, Feaver JL, Stoykovich MP. Network connectivity and long-range continuity of lamellar morphologies in block copolymer thin films. Macromolecules. 2012;**45**: 1587-1594. DOI: 10.1021/ma2025336

[14] Ruiz R, Sandstrom RL, Black CT. Induced orientational order in symmetric diblock copolymer thin films. Advanced Materials. 2007;**19**: 587-591. DOI: 10.1002/adma.200600287

[15] Yang T, Tian SW, Zhu Y, Li WH. Perfectly ordered patterns formed by a heterogeneous nucleation process of block copolymer self-assembly under rectangular confinement. Langmuir. 2016;**32**:13787-13794. DOI: 10.1021/acs.langmuir.6b03638

[16] Yang T, Zhu Y, Xue HY, Li WH. Defect patterns from controlled heterogeneous nucleations by polygonal confinements. Langmuir. 2018;**34**:

5901-5909. DOI: 10.1021/acs.langmuir.8b00101

[17] Li WH, Müller M. Directed self-assembly of block copolymers by chemical or topographical guiding patterns: Optimizing molecular architecture, thin-film properties, and kinetics. Progress in Polymer Science. 2016;**54–55**:47-75. DOI: 10.1016/j.progpolymsci.2015.10.008

[18] Xu Y, Xie N, Li W, Qiu F, Shi AC. Phase behaviors and ordering dynamics of diblock copolymer self-assembly directed by lateral hexagonal confinement. The Journal of Chemical Physics. 2012;**137**:194905. DOI: 10.1063/1.4765098

[19] Cheng JY, Rettner CT, Sanders DP, Kim HC, Hinsberg WD. Dense self-assembly on sparse chemical patterns: Rectifying and multi-plying lithographic patterns using block copolymers. Advanced Materials. 2008;**20**:3155-3158. DOI: 10.1002/adma.200800826

[20] Tavakkoli AKG, Gotrik KW, Hannon AF, Alexander-Katz A, Ross CA, Berggren KK. Templating three-dimensional self-assembled structures in bilayer block copolymer films. Science. 2012;**336**:1294-1298. DOI: 10.1126/science.1218437

[21] Li WH, Qiu F, Yang YL, Shi AC. Ordering dynamics of directed self-assembly of block copolymers in periodic two-dimensional fields. Macromolecules. 2010;**43**:1644-1650. DOI: 10.1021/ma9023203

[22] Li WH, Xie N, Qiu F, Yang YL, Shi AC. Ordering kinetics of block copolymers directed by periodic two-dimensional rectangular fields. The Journal of Chemical Physics. 2011;**134**:144901. DOI: 10.1063/1.3572266

[23] Xie N, Li WH, Qiu F, Shi AC. New strategy of nanolithography via controlled block copolymer self-assembly. Soft Matter. 2013;**9**:536-542. DOI: 10.1039/c2sm26833g

[24] Deng HL, Xie N, Li WH, Qiu F, Shi AC. Perfectly ordered patterns via corner-induced heterogeneous nucleation of self-assembling block copolymers confined in hexagonal potential wells. Macromolecules. 2015;**48**:4174-4182. DOI: 10.1021/acs.macromol.5b00681

[25] Kim SO, Solak HH, Stoykovich MP, Ferrier NJ, de Pablo JJ, NealeyPF. Epitaxial self-assembly of block copolymers on lithographically defined nanopatterned substrates. Nature. 2003;**424**:411-414. DOI: 10.1038/nature01775

[26] Ruiz R, Kang HM, Detcheverry FA, Dobisz E, Kercher DS, Albrecht TR, et al. Density multiplication and improved lithography by directed block copolymer assembly. Science. 2008;**321**:936-939. DOI: 10.1126/science.1157626

[27] Segalman RA, Yokoyama H, Kramer EJ. Graphoepitaxy of spherical domain block copolymer films. Advanced Materials. 2001;**13**:1152-1155. DOI: 10.1002/1521-4095(200108)13:15<1152::AID-ADMA1152>3.0.CO;2-5

[28] Cheng JY, Mayes AM, Ross CA. Nanostructure engineering by templated self-assembly of block copolymers. Nature Materials. 2004;**3**:823-828. DOI: 10.1038/nmat1211

[29] Matsen MW, Schick M. Stable and unstable phases of a diblock copolymer melt. Physical Review Letters. 1994;**72**:2660-2663. DOI: 10.1103/PhysRevLett.72.2660

[30] Matsen MW. The standard Gaussian model for block copolymer melts. Journal of Physics. Condensed Matter. 2002;**14**:R21-R47. DOI: 10.1088/0953-8984/14/2/201

[31] Tyler CA, Morse DC. Orthorhombic Fddd network in triblock and diblock

copolymer melts. Physical Review Letters. 2005;**94**:208302. DOI: 10.1103/PhysRevLett.94.208302

[32] Liu CC, Ramirez-Hernandez A, Han E, Craig GSW, Tada Y, Yoshida H, et al. Chemical patterns for directed self-assembly of lamellae-forming block copolymers with density multiplication of features. Macromolecules. 2013;**46**: 1415-1424. DOI: 10.1021/ma302464n

[33] Tada Y, Akasaka S, Takenaka M, Yoshida H, Ruiz R, Dobisz E, et al. Nine-fold density multiplication of hcp lattice pattern by directed self-assembly of block copolymer. Polymer. 2009;**50**: 4250-4256. DOI: 10.1016/j.polymer.2009.06.039

[34] Hashimoto T, Sakamoto N, Koga T. Nucleation and growth of anisotropic grain in block copolymers near order–disorder transition. Physical Review E. 1996;**54**:5832-5835. DOI: 10.1103/PhysRevE.54.5832

[35] Wickham RA, Shi AC, Wang ZG. Nucleation of stable cylinders from a metastable lamellar phase in a diblock copolymer melt. The Journal of Chemical Physics. 2003;**118**: 10293-10305. DOI: 10.1063/1.1572461

[36] Kalikmanov VI. Nucleation theory. Lecture Notes in Physics. 2012;**860**: 17-53. DOI: 10.1007/978-90-481-3643-8

[37] Spencer RKW, Wickham RA. Simulation of nucleation dynamics at the cylinder-to-lamellar transition in a diblock copolymer melt. Soft Matter. 2013;**9**:3373-3382. DOI: 10.1039/C3SM27499C

[38] Ohta T, Ito A. Dynamics of phase-separation in copolymer-homopolymer mixtures. Physical Review E. 1995;**52**: 5250-5260. DOI: 10.1103/PhysRevE.52.5250

[39] Ohta T, Kawasaki K. Equilibrium morphology of block copolymer melts. Macromolecules. 1986;**19**:2621-2632. DOI: 10.1021/ma00164a028

[40] Tang QY, Ma YQ. High density multiplication of graphoepitaxy directed block copolymer assembly on two-dimensional lattice template. Soft Matter. 2010;**6**:4460. DOI: 10.1039/c0sm00238k

[41] Krishnan MR, Lu KY, Chiu WY, Chen IC, Lin JW, Lo TY, et al. Directed self-assembly of star-block copolymers by topographic nanopatterns through nucleation and growth mechanism. Small. 2018;**14**:1704005. DOI: 10.1002/smll.201704005

[42] Harrison C, Angelescu DE, Trawick M, Cheng ZD, Huse DA, Chaikin PM, et al. Pattern coarsening in a 2D hexagonal system. EPL. 2004;**67**: 800-806. DOI: 10.1209/epl/i2004-10126-5

[43] Vega DA, Harrison CK, Angelescu DE, Trawick ML, Huse DA, Chaikin PM, et al. Ordering mechanisms in two-dimensional sphere-forming block copolymers. Physical Review E. 2005;**71**: 061803. DOI: 10.1103/PhysRevE.71.061803

[44] Gómez LR, Vallés EM, Vega DA. Lifshitz-Safran coarsening dynamics in a 2D hexagonal system. Physical Review Letters. 2006, 2006;**97**:188302. DOI: 10.1103/PhysRevLett.97.188302

[45] Pezzutti AD, Vega DA, Villar MA. Dynamics of dislocations in a two-dimensional block copolymer system with hexagonal symmetry. Philosophical Transactions. Series A, Mathematical, Physical, and Engineering Sciences. 2011;**369**:335-350. DOI: 10.1098/rsta.2010.0269